Chemical Geology 347 (2013) 190–198

Contents lists available at SciVerse ScienceDirect

Chemical Geology

journal homepage: www.elsevier.com/locate/chemgeo

Prior calcite precipitation and source mixing process influence Sr/Ca, Ba/Ca and $^{87}Sr/^{86}Sr$ of a stalagmite developed in southwestern Japan during 18.0 4.5 ka

Masako Hori [a,*], Tsuyoshi Ishikawa [b], Kazuya Nagaishi [c], Ke Lin [d], Bo-Shian Wang [a], Chen-Feng You [a], Chuan-Chou Shen [d], Akihiro Kano [e]

[a] Earth Dynamic System Research Center, National Cheng Kung University, No. 1, University Road, Tainan, 701, Taiwan
[b] Kochi Institute for Core Sample Research, Japan Agency for Marine-Earth Science and Technology (JAMSTEC), 200 Monobe Otsu, Nankoku City, Kochi, 783-8502, Japan
[c] Marine Works Japan Ltd., 200 Monobe Otsu, Nankoku City, Kochi, 783-8502, Japan
[d] High-precision Mass Spectrometry and Environment Change Laboratory (HISPEC), National Taiwan University, No. 1, Section 4, Roosevelt Road, Taipei, 10617, Taiwan
[e] Faculty of Social and Cultural Studies, Kyushu University, 744 Motooka, Nishi-Ku, Fukuoka City, Fukuoka, 819-0395, Japan

ARTICLE INFO

Article history:
Received 20 August 2012
Received in revised form 9 March 2013
Accepted 12 March 2013
Available online 24 March 2013

Editor: U. Brand

Keywords:
Stalagmite
Sr isotopes
Prior calcite precipitation
Holocene

ABSTRACT

We measured Sr/Ca, Ba/Ca, $^{87}Sr/^{86}Sr$ ratios, $\delta^{18}O$ and $\delta^{13}C$ values in a stalagmite, which developed 18.0–4.5 thousand years ago (ka) in southwestern Japan. Dripwater and two major bedrocks (limestone and andesite) in the locality were also studied. The $^{87}Sr/^{86}Sr$ ratios of the stalagmite are relatively homogeneous (0.706852–0.706921), suggesting a steady source mixing ratio of ~40% from high-$^{87}Sr/^{86}Sr$ limestone and ~60% from low-$^{87}Sr/^{86}Sr$ andesite. The stalagmite Sr/Ca and Ba/Ca ratios were higher than the ratio expected from the dissolved fraction of limestone and andesite. The covariance among Sr/Ca, Ba/Ca, and $\delta^{13}C$ profiles suggests a significant role of prior calcite precipitation (PCP), i.e., carbonate precipitation from infiltrating water before the water drips on a stalagmite. The relationships among stalagmite Sr/Ca, Ba/Ca ratios and $\delta^{13}C$ values are consistent with the Rayleigh-type fractionation model, supporting that PCP results in successive enrichment of Sr, Ba and ^{13}C in the aqueous phase and the resulting stalagmite. The degree of PCP calculated for the stalagmite is highly variable from 0 to 85%, and generally decreased from the last glacial period to the middle Holocene. The large degree of PCP observed during 18–15 ka implies a relatively dry climate during this period, which is consistent with weak monsoon intensity inferred by the $\delta^{18}O$ values. The $^{87}Sr/^{86}Sr$ ratios of the stalagmite show a slight decrease through the entire period. The increase in the andesite-derived fraction with relatively high $^{87}Sr/^{86}Sr$ may result from accelerated silicate weathering in the epikarst with increasing temperature, humidity, and soil pCO_2.

1. Introduction

Geochemical proxies in stalagmites are important archives for understanding terrestrial paleoclimates. One of the most successful proxies is oxygen isotopes ($\delta^{18}O$). Oxygen isotope ratios have been used to reconstruct paleo-temperature and rainfall properties, such as amount, seasonality, and moisture sources (e.g., McDermott, 2004; Fairchild et al., 2006). For instance, studies of stalagmite $\delta^{18}O$ in southern China have shown that the strength of the East Asian summer monsoon responds to changes in Northern Hemisphere summer insolation (Wang et al., 2001, 2008). These studies often rely on the amount effect (Dansgaard, 1964) with regard to rainfall $\delta^{18}O$ values, although speleothem $\delta^{18}O$ values are influenced by a complex of processes in the atmosphere, epikarst and cave (e.g., Lachniet, 2009). Measuring multiple proxies should be a valuable approach for understanding the relationships among interacting processes and their influence.

Other valuable proxies in stalagmites include the trace elements. The alkaline-earth metals (Me), especially Mg and Sr, have been used as paleothermometers in marine carbonates (e.g., Nümberg et al., 1996; Shen et al., 1996). Compared with marine systems, where the Me/Ca ratio in water can be considered as a constant, cave or karst systems involve numerous processes that influence the Me/Ca ratio during mineral dissolution and precipitation (Fairchild et al., 2000; Tooth and Fairchild, 2003; Fairchild and Treble, 2009). Therefore, a constant Me/Ca ratio in dripwater is not likely throughout long time intervals.

One of the important processes controlling the Me/Ca ratio in stalagmites is prior calcite precipitation (PCP), where carbonate precipitates from infiltrating water upstream of the dripping point (Fairchild et al., 2000). In the case of alkaline-earth metals having a carbonate/water distribution coefficient much smaller than unity, PCP increases the Me/Ca ratio of both dripwater and the stalagmite. Because PCP is related to CO_2 degassing from the infiltrating water, this process is

* Corresponding author at: Atmosphere and Ocean Research Institute, the University of Tokyo, Kashiwa-no-ha 5-1-5, Kashiwa City, Chiba, 277-8564, Japan.
E-mail address: horizon@aori.u-tokyo.ac.jp (M. Hori).

0009-2541/$ – see front matter © 2013 Elsevier B.V. All rights reserved.
http://dx.doi.org/10.1016/j.chemgeo.2013.03.005

enhanced during dry periods when the water slowly descends in aerated channels in the limestone aquifer (Fairchild et al., 2000; McDermott, 2004). The stalagmite Me/Ca ratio changes with humidity, when PCP principally controls the Me/Ca ratio.

However, the Me/Ca ratios of water and stalagmites also vary with the mixing of different sources of dissolved metals. In the simplest case, there are two sources for dissolved cations: Ca-enriched limestone and an inter-karst or exotic Me-enriched source such as silicate wallrock, soil or aeolian dust. The relative proportion of the two sources controls the Me/Ca ratios in dripwater (Fairchild et al., 2006). Because the isotopic signature does not change with the degree of PCP, isotopic measurements of the relevant metal can identify sources and quantify mixing ratios of metallic cation. Strontium isotope ratios are used in this approach because the ratio ($^{87}Sr/^{86}Sr$) varies predictably among different sources. Previous studies using Sr isotope ratios in stalagmites have focused on the contribution of different Sr sources (e.g., Banner et al., 1996; Goede et al., 1998; Ayalon et al., 1999; Zhou et al., 2009).

In this study, we investigated Sr sources in a stalagmite growing from the last glacial time to middle Holocene (18.0–4.5 ka) in southwestern Japan. We first identify the Sr sources and evaluate the source mixing process using the $^{87}Sr/^{86}Sr$ ratios of bedrock in the catchment area. We evaluate the degree of PCP based on Sr/Ca and Ba/Ca ratios and $\delta^{13}C$ in the stalagmite. Finally, the age profiles of these proxies are used for interpreting trends in climate during the growth period of the stalagmite.

2. Materials and methods

2.1. Sample locality and materials

A 13-cm-long clear stalagmite, Hiro-1, was collected from the Maboroshi cave (elevation 450 m; 34°49′ N, 133°13′ E) in northeast Hiroshima Prefecture, southwestern Japan (Fig. 1a). The cave, located at the southern foot of the Chugoku Mountains, was first discovered in 1992. The cave is nearly horizontal with currently-explorable length of 740 m. The site of Hiro-1 is 150 m from the cave entrance at 350 m in altitude. The deepest part of the passage between this site and the entrance used to be blocked with muddy sediments until exploration in 1993. Therefore, the ventilation in the cave was likely limited.

The limestone plateau containing the Maboroshi cave is a part of the Akiyoshi Terrane of Carboniferous–Permian age. The limestone was deposited on a Lower Carboniferous basaltic seamount and later intruded by Cretaceous andesite (Fig. 1b), which is distributed in the catchment area and within the cave. The annual average temperature from the nearest meteorological observatory, Yuki (elevation 510 m; 34°47′ N, 133°16′ E), is 10.7 °C (1988–2007). The mean annual rainfall is 1296 mm. The catchment area is characterized by conifer-dominated forest that covers soils of one to several meters in thickness. Soil includes limestone and andesite gravel, and consists of weathered andesite, insoluble limestone residue, and possibly aeolian sediments. However, the contribution of pyroclastic material is likely minor because there is no visible ash bed in the Holocene cover in this locality. The Chugoku Mountains include only one active volcano, andesitic Mt. Sambe located ~60 km WNW from the cave. The stalagmite consists of clear calcite crystals, and the carbonate Sr/Ca and $^{87}Sr/^{86}Sr$ were most likely inherited from the dissolved components of the dripwater.

Thirty four horizons of Hiro-1 were ^{230}Th-dated following the methods in Shen et al. (2002, 2003, 2012) with an uncertainty of 0.3–1.1% (2RSD). According to the dating results, the growth interval of the stalagmite is from 18.1 to 4.5 ka (Table 1). The record includes two hiatuses in 10.8–7.7 ka (Hiatus 1) and in 12.8–11.4 ka (Hiatus 2). Hiatus 2 would correspond to the Younger Dryas (YD, Alley et al., 1993). Paleoclimatic reconstruction has been carried out using $\delta^{18}O$ profiles from the same stalagmite for the interval 15.5–10.7 ka, which showed synchronous trends with $\delta^{18}O$ profiles from Chinese caves and Greenland ice cores (Shen et al., 2010). In this study, we present trace element and stable isotope data for the entire growth interval of the stalagmite.

Three grayish limestone specimens (A, B, and C) and three greenish andesite specimens (AN1, AN2 and AN3) were collected from the catchment area. Dripwater was collected in pre-cleaned 10-L polyethylene containers and in 15 mL glass vials at two sites (DW1 and DW2) near the stalagmite sampling point from 13 to 20 November 2009. The drip rate at the DW1 site was approximately 1 L/day, faster than at the DW2 site (~1 L/week). The dripwater samples collected in 10-L polyethylene containers were acidified with ultrapure HNO_3 to prevent mineral precipitation during storage.

2.2. $\delta^{18}O$ and $\delta^{13}C$ analysis

Powdered sub-samples (300 μg) for $\delta^{18}O$ and $\delta^{13}C$ analyses were collected at 0.2-mm spaced intervals along the stalagmite growth axis using a dental drill. The samples were converted into carbon dioxide by reaction with phosphoric acid. Oxygen and carbon isotopic ratios were measured on an isotope ratio mass spectrometer, Finnigan MAT Delta Plus, combined with an on-line preparation and introduction system, GAS BENCH, at Kyushu University. The $\delta^{18}O$ and $\delta^{13}C$ values are expressed using the conventional δ notation with respect to Vienna Pee Dee Belemnite (VPDB). Repeated measurements of a laboratory standard (powdered Jurassic limestone at Solnhofen, Germany) calibrated with NBS-19 gave analytical reproducibility better than 0.22‰ for $\delta^{18}O$ and 0.19‰ for $\delta^{13}C$ (2SD) (Hori et al., 2009).

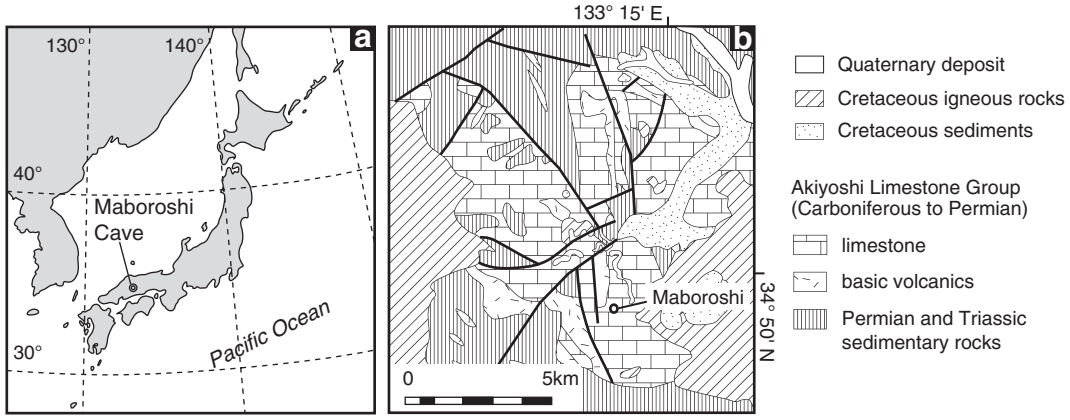

Fig. 1. (a) Location of the Maboroshi cave in southwest Japan. (b) Geological map of the study area.

Table 1
U–Th dating results of Hiro-1. Dating error is given in 2SD.

Depth mm	Weight g	^{238}U ppb	^{232}Th ppt	δ^{234}U measured[a]	$\delta^{234}U_{initial}$ corrected [b]	[^{230}Th/^{238}U] activity	[^{230}Th/^{232}Th] ppm[c]	Age uncorrected	Age corrected[d]
2.0	0.2113	694.8 ± 0.8	155 ± 2	906 ± 2	918 ± 2	0.0788 ± 0.0005	5847 ± 76	4594 ± 32	4533 ± 32
8.4	0.0602	749.3 ± 0.9	42 ± 6	874 ± 3	886 ± 3	0.0808 ± 0.0004	23,673 ± 3246	4796 ± 23	4737 ± 23
18.8	0.0567	794.0 ± 0.9	219 ± 6	887 ± 3	901 ± 3	0.0906 ± 0.0004	5437 ± 155	5354 ± 26	5292 ± 26
27.8	0.0463	606.0 ± 1.3	51 ± 8	867 ± 5	881 ± 5	0.0999 ± 0.0007	19,705 ± 2924	5984 ± 45	5925 ± 45
37.8	0.0529	543.2 ± 0.8	19 ± 7	877 ± 4	893 ± 4	0.1062 ± 0.0007	49,116 ± 16,673	6331 ± 44	6272 ± 44
40.0	0.0572	723.1 ± 0.8	36 ± 6	875 ± 3	891 ± 3	0.1060 ± 0.0005	35,212 ± 5964	6331 ± 30	6272 ± 30
47.0	0.0576	282.7 ± 0.4	5 ± 6	861 ± 3	877 ± 3	0.1106 ± 0.0009	100,252 ± 117,694	6660 ± 58	6601 ± 58
53.8	0.0482	472.7 ± 0.6	28 ± 7	865 ± 3	884 ± 3	0.1306 ± 0.0008	36,855 ± 9633	7884 ± 49	7825 ± 49
56.8	0.0478	580.8 ± 0.9	3030 ± 10	864 ± 4	891 ± 4	0.1778 ± 0.0009	563 ± 3	10,864 ± 60	10,733 ± 70
58.6	0.0388	244.3 ± 0.4	21 ± 9	860 ± 4	886 ± 4	0.1738 ± 0.0018	34,087 ± 14,880	10,636 ± 115	10,577 ± 115
60.8	0.0576	381.0 ± 0.6	509 ± 21	870 ± 4	897 ± 4	0.1784 ± 0.0009	2207 ± 92	10,870 ± 63	10,793 ± 64
60.8	0.0457	348.3 ± 0.2	216 ± 8	860 ± 2	887 ± 2	0.1769 ± 0.0012	4707 ± 169	10,830 ± 76	10,764 ± 76
62.4	0.0350	459.6 ± 0.3	222 ± 10	852 ± 2	879 ± 2	0.1794 ± 0.0010	6131 ± 280	11,043 ± 66	10,978 ± 66
64.6	0.0384	241.0 ± 0.2	3 ± 9	840 ± 3	867 ± 3	0.1812 ± 0.0016	237,256 ± 707,877	11,231 ± 106	11,173 ± 106
65.0	0.0452	286.6 ± 0.4	59 ± 8	838 ± 4	865 ± 4	0.1840 ± 0.0012	14,856 ± 1956	11,433 ± 84	11,372 ± 84
65.8	0.0328	432.2 ± 0.3	21 ± 11	828 ± 3	858 ± 3	0.2020 ± 0.0012	69,869 ± 35,941	12,682 ± 82	12,623 ± 82
68.8	0.0453	407.3 ± 0.7	37 ± 8	822 ± 4	853 ± 4	0.2055 ± 0.0010	37,439 ± 7796	12,953 ± 71	12,894 ± 71
69.8	0.0373	391.4 ± 0.4	97 ± 9	832 ± 3	864 ± 3	0.2118 ± 0.0012	14,181 ± 1374	13,296 ± 82	13,234 ± 82
71.6	0.0450	455.4 ± 0.5	6 ± 8	845 ± 3	878 ± 3	0.2175 ± 0.0011	291,106 ± 400,907	13,571 ± 78	13,513 ± 78
73.6	0.0393	515.5 ± 0.6	8 ± 9	837 ± 3	869 ± 3	0.2167 ± 0.0012	223,042 ± 238,866	13,583 ± 82	13,525 ± 82
74.8	0.0635	426.6 ± 0.6	18 ± 6	832 ± 3	864 ± 4	0.2177 ± 0.0008	84,444 ± 25,507	13,692 ± 62	13,633 ± 62
75.2	0.0458	401.4 ± 0.4	3 ± 8	834 ± 3	867 ± 3	0.2170 ± 0.0011	425,831 ± 958,292	13,620 ± 75	13,562 ± 75
77.2	0.0526	533.9 ± 0.9	17 ± 7	853 ± 4	889 ± 4	0.2317 ± 0.0008	118,836 ± 45,739	14,443 ± 62	14,385 ± 62
78.6	0.0396	604.8 ± 0.4	466 ± 9	849 ± 2	885 ± 2	0.2359 ± 0.0009	5056 ± 98	14,758 ± 65	14,689 ± 65
81.0	0.0632	640.2 ± 1.2	104 ± 6	866 ± 4	905 ± 4	0.2516 ± 0.0010	25,509 ± 1388	15,647 ± 74	15,587 ± 74
81.0	0.0477	701.4 ± 0.5	137 ± 7	865 ± 2	904 ± 2	0.2510 ± 0.0008	21,210 ± 1133	15,611 ± 58	15,550 ± 58
82.6	0.0407	775.6 ± 0.5	12 ± 9	808 ± 2	845 ± 2	0.2461 ± 0.0008	264,192 ± 189,410	15,809 ± 56	15,751 ± 56
84.6	0.0540	707.8 ± 1.1	49 ± 6	814 ± 4	852 ± 4	0.2489 ± 0.0009	59,665 ± 7891	15,942 ± 74	15,883 ± 74
89.8	0.0425	958.2 ± 0.8	2 ± 8	835 ± 2	875 ± 2	0.2561 ± 0.0009	1,925,316 ± 7,492,116	16,230 ± 62	16,172 ± 62
97	0.0418	1160.4 ± 1.6	51 ± 8	817 ± 3	857 ± 3	0.2606 ± 0.0008	98,967 ± 16,344	16,713 ± 60	16,654 ± 60
102.2	0.0514	1021.4 ± 0.7	88 ± 7	811 ± 2	850 ± 2	0.2603 ± 0.0007	50,082 ± 3873	16,760 ± 51	16,701 ± 51
109.6	0.0510	1033.5 ± 1.7	185 ± 7	807 ± 4	847 ± 5	0.2631 ± 0.0007	24,290 ± 901	16,987 ± 67	16,926 ± 67
118.6	0.0448	1364.1 ± 2.0	177 ± 8	878 ± 5	922 ± 5	0.2771 ± 0.0007	35,304 ± 1557	17,217 ± 66	17,157 ± 66
127.2	0.0566	828.7 ± 1.5	192 ± 6	825 ± 5	868 ± 5	0.2828 ± 0.0008	20,152 ± 648	18,160 ± 78	18,098 ± 78

Age (before AD1950) corrections were made using a ^{230}Th/^{232}Th atomic ratio of 4 ± 2 ppm.

[a] $\delta^{234}U = ([^{234}U/^{238}U]_{activity} - 1) \times 1000$.

[b] $\delta^{234}U_{initial}$ corrected was calculated based on ^{230}Th age (T), i.e., $\delta^{234}U_{initial} = \delta^{234}U_{measured}\, xe^{\lambda 234 * T}$, and T is corrected age.

[c] The degree of detrital ^{230}Th contamination is indicated by the [^{230}Th/^{232}Th] atomic ratio instead of the activity ratio.

[d] $[^{230}Th/^{238}U]_{activity} = 1 - e^{-\lambda 230T} + (\delta^{234}U / 1000)[\lambda_{230} / (\lambda_{230} - \lambda_{234})](1 - e^{-(\lambda 230 - \lambda 234)T})$, where T is the age. Decay constants are 9.1577×10^{-6} yr^{-1} for ^{230}Th, 2.8263×10^{-6} yr^{-1} for ^{234}U (Cheng et al., 2000), and 1.55125×10^{-10} yr^{-1} for ^{238}U (Jaffey et al., 1971).

Stalagmite Hiro-1 δ^{18}O data passed the Hendy Test (Hendy, 1971) with coeval subsamples at four depths at 56.6, 57.6, 67.7, and 77.8 mm in our previous study (Shen et al., 2010) and additional three depths at 10.2, 110.9, and 122.5 mm (Appendix A). The δ^{13}C values in limestone samples near the cave were analyzed with the same methods.

2.3. Sr/Ca and Ba/Ca ratios

Stalagmite sub-samples (1–7 mg) were collected at approximately 2-mm intervals for measuring Sr/Ca and Ba/Ca ratios. These samples were dissolved in 5-mL 0.15 M HNO_3 containing 10-ppb indium internal standard. An aliquot of 0.1 mL was then diluted ten-fold for elemental analysis by quadrupole ICP-MS (Perkin Elmer, Elan DRCII) at the Kochi Core Center (KCC) and High Resolution ICP-MS (Thermo Fisher ELEMENT 2) at National Cheng Kung University (NCKU). The remaining 4.9 mL was used for Sr isotopic analysis (Section 2.4). Standards of 0, 1, 5 and 10 ppb were prepared using multi element standards (SPEX CLMS-1 and 2, SPEX CertiPrep Inc.). Instrumental bias was corrected using a 10 ppb indium internal standard. Analytical reproducibility for Sr/Ca and Ba/Ca was evaluated by repeated analysis of a carbonate standard (JCp-1, Geological Survey of Japan), and was better than 4.5% (2RSD, n = 6). For the host limestone samples, powdered sub-samples of 6–16 mg were treated and measured with the same procedure.

We also analyzed Sr/Ca and Ba/Ca ratios of soluble components of the andesite samples following the methods described by Yokoo et al. (2004). Andesite samples of 1–2 g were crushed into chips of 3- to 5-mm in diameter, and were first soaked with 5 mL of Milli-Q water for 5 min at room temperature. A 2-mL aliquot of the leachate was filtered using a 1 μm membrane filter to obtain H_2O-leachate. 30% acetic acid (HOAc) was added to each andesite sample containing 3-mL water to adjust the HOAc concentration to 5%, and the sample was soaked at 75 °C for 2 h. The 2-mL filtrate (HOAc-leachate) was collected from each sample. Both leachates were dried and dissolved in 2 mL of 0.15 M HNO_3 containing 10-ppb indium. The HOAc-leachate was further diluted 100-fold for ICP-MS analysis. The remaining leachate was used for Sr isotopic analysis.

Calcium concentration in the dripwater samples collected in glass vials was analyzed by ion chromatography after 3-fold dilution. Trace elements were analyzed by ICP-MS after 10-fold dilution.

2.4. $^{87}Sr/^{86}Sr$ ratios

For Sr separation with an ion-exchange resin column (0.2 mL Eichrom Sr resin; Horwitz et al., 1992), the NO_3^- concentration of sample solutions was adjusted to 3 M using 68% HNO_3. The resin column was pre-cleaned and conditioned with 3 M HNO_3. After loading the sample solution, 3-mL 3 M HNO_3 was added to the column to elute cations such as Ca, Ba and Rb. The Sr fraction was collected by adding 2-mL of 0.05 M HNO_3. Procedural Sr blanks during the column separation procedure contained less than <0.6 ng Sr, which is insignificant for isotopic analysis using 100–150 ng Sr.

Sr isotopic compositions were measured by thermal ionization mass spectrometer (Thermo Finnigan Triton) using a tungsten single filament method with tantalum oxide activator (at KCC) or a tantalum–rhenium double filament method (at NCKU). In both cases, 100–

150 ng of Sr in 0.8–1.0 μL solution was dried on an evaporation filament. During the measurement, the intensity of ^{88}Sr ion signal was maintained near 4×10^{11} A. The low ^{85}Rb signal ensured that the interference of ^{87}Rb on ^{87}Sr signal was insignificant (<0.1%) for all analyses. 140 cycles of data were acquired in a single run. Instrumental bias was corrected using NIST987 standard (Table 2), which was normalized to 0.710240. Analytical reproducibility was ascertained by repeated measurements of JCp-1 as 0.709164 ± 0.000008 (2SD, n = 9) at KCC and 0.709168 ± 0.000019 (2SD, n = 5) at NCKU.

3. Results

3.1. Hiro-1

3.1.1. $\delta^{18}O$ and $\delta^{13}C$ profiles

$\delta^{18}O$ values of Hiro-1 vary between −8.2 and −5.2‰ (Fig. 2). The values are generally high (−7.1 to −5.2‰) in the cold Heinrich stadial 1 (HS1, 17.5–14.5 ka, Broecker and Barker, 2007; Barker et al., 2009). A distinct negative shift of 1.4‰ is evident around 14.6 ka, which corresponds to the onset of the Bølling–Allerød warming, likely reflecting an intensified Asian summer monsoon or an increase in temperature (Shen et al., 2010). Rapid increases in $\delta^{18}O$ values are observed across the two hiatuses at 12.6 to 11.4 ka and 10.7 and 7.8 ka (Hiatus 2 and Hiatus 1, respectively). Excluding these changes, $\delta^{18}O$ values generally decrease from the Bølling–Allerød (around −6.5‰) to the middle Holocene (around −7.5‰).

$\delta^{13}C$ values vary between −9.9 and −2.9‰ (Fig. 2). Elevated $\delta^{13}C$ values (about −3.5‰) are recorded around 18 ka. The $\delta^{13}C$ values decrease to −7‰ at 16 ka, and again increase to −5‰ at the end of HS1. An abrupt shift of 3‰ was recorded across the onset of the Bølling−Allerød. The $\delta^{13}C$ profile also shows a sharp increase across the two hiatuses, which is a similar pattern to the $\delta^{18}O$ values. The $\delta^{13}C$ values then decrease toward 6.6 ka, where the minimum value (−9.9‰) occurs, and gradually increases to −6.7‰ at the middle Holocene (Fig. 2).

3.1.2. Sr/Ca, Ba/Ca and $^{87}Sr/^{86}Sr$ ratios

The Sr/Ca ratio decreases from 17.7 ka (maximum 0.86 mmol/mol) to 11.3 ka (0.18). During the remaining period, Sr/Ca ratios generally range from 0.15 to 0.41 mmol/mol (Fig. 3 and Table 3). A sharp increase in Sr/Ca from 0.2 to 0.4 mmol/mol occurs at 11.4–10.8 ka between Hiatus 1 and Hiatus 2 (Fig. 3). The pattern for the Ba/Ca ratio is similar to the pattern for the Sr/Ca ratio ($R^2 = 0.86$; Fig. 3). The maximum Ba/Ca (25 μmol/mol) is found at 17.7 ka and the minimum Ba/Ca (3.6 μmol/mol) occurs at 4.6 ka (the stalagmite top).

Table 2
Measured $^{87}Sr/^{86}Sr$ values of NIST987 at Kochi Core Center (KCC) and National Cheng Kung University (NCKU).

		$^{87}Sr/^{86}Sr$	2SE (×10^{-6})
KCC	NIST987	0.710257	±7.4
	NIST987	0.710265	±6.8
	NIST987	0.710258	±7.0
	NIST987	0.710255	±6.6
	NIST987	0.710253	±6.8
	NIST987	0.710259	±7.2
	NIST987	0.710259	±6.4
	NIST987	0.710262	±7.4
	NIST987	0.710256	±6.8
	NIST987	0.710261	±6.6
	NIST987	0.710262	±6.2
	NIST987	0.710261	±6.0
	NIST987	0.710261	±6.6
	NIST987	0.710263	±7.2
	NIST987	0.710265	±7.4
	NIST987	0.710263	±6.8
NCKU	NIST987	0.710207	±19
	NIST987	0.710209	±14

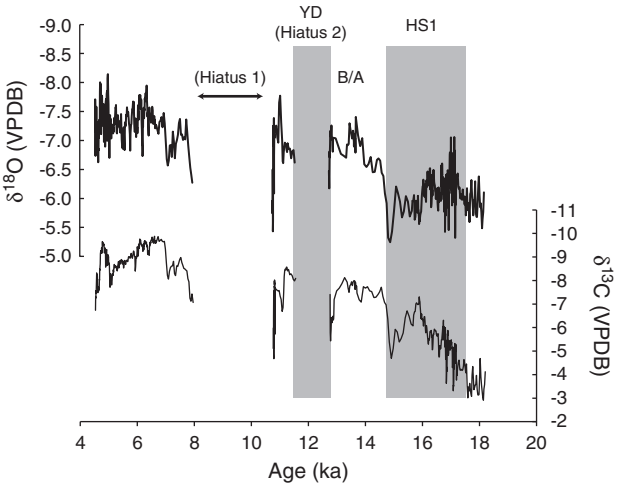

Fig. 2. Age profiles for oxygen and carbon isotopes in the stalagmite Hiro-1, Maboroshi Cave, Japan.

The $^{87}Sr/^{86}Sr$ ratio generally decreases from 0.70690 to 0.70687 throughout the growth period (Table 3 and Fig. 3). Some outlying values are observed, including the maximum value (0.706921) at 13.4 ka and the minimum value (0.706852) at 6.7 ka. The general decrease in $^{87}Sr/^{86}Sr$ with age is shown by the correlation between $^{87}Sr/^{86}Sr$ ratio and age ($R^2 = 0.44$ for all data and $R^2 = 0.69$ excluding two outliers). In addition, the difference of the $^{87}Sr/^{86}Sr$ ratio between two intervals before Hiatus 2 (0.706894 ± 0.000020) and after Hiatus 1 (0.706880 ± 0.000020) was confirmed by the rejected null hypothesis ($p < 0.01$). The $^{87}Sr/^{86}Sr$ ratio slightly decreases at 5.7 ka by 0.00015, and then gradually increases by 0.00010.

3.2. Bedrock and dripwater samples

The Sr/Ca ratios of the three limestone samples range from 0.11 to 0.19 mmol/mol (Table 4), and the average is 0.15 mmol/mol. The Ba/Ca ratios for the limestones are in a narrow range of 5.5–7.5 μmol/mol with an average of 6.4 μmol/mol. The $^{87}Sr/^{86}Sr$ ratios range between 0.707422 and 0.707830 with an average of 0.707601, which is distinctly

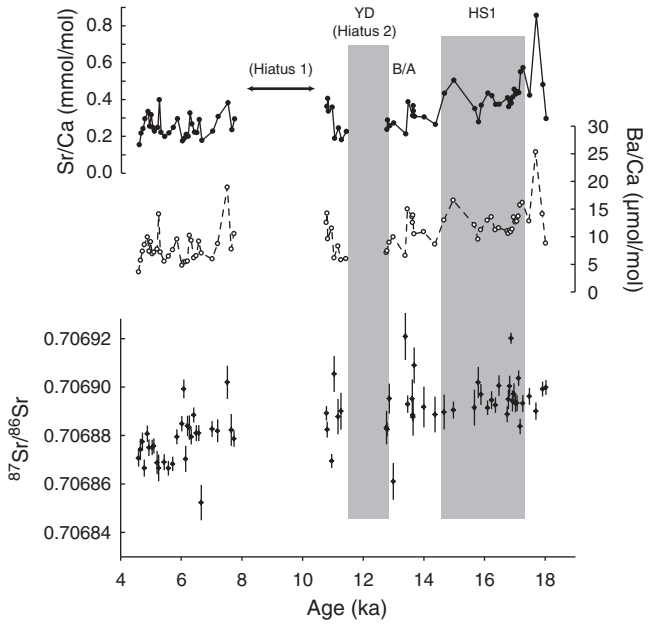

Fig. 3. Age profiles for Sr/Ca, Ba/Ca molar fraction ratios, $^{87}Sr/^{86}Sr$ ratios and $\delta^{18}O$ values in Hiro-1.

Table 3
$\delta^{13}C$ values, Sr/Ca and Ba/Ca molar fraction ratios and $^{87}Sr/^{86}Sr$ ratio in Hiro-1.

depth from the top (cm)	Calendar age (years BP)	$\delta^{13}C$[a] (‰ VPDB)	Sr/Ca mmol/mol	Ba/Ca μmol/mol	$^{87}Sr/^{86}Sr$	2SE ($\times10^{-6}$)	[b]
0.20	4591	−8.16	0.15	3.6	0.706871	±7.0	1
0.40	4655	−7.70	0.22	5.7	0.706874	±8.8	1
0.60	4719	−9.27	0.24	7.4	0.706878	±7.6	1
0.80	4782	−9.51	0.30	8.6	0.706867	±7.0	1
1.00	4881	−9.27	0.33	9.9	0.706881	±6.8	1
1.10	4934	−8.84	0.26	7.4	0.706875	±6.8	1
1.20	4987	−9.02	0.32	9.1	–	–	
1.30	5041	−7.72	0.25	6.9	0.706875	±6.4	1
1.40	5094	−7.82	0.23	7.2	0.706876	±6.2	1
1.60	5201	−8.63	0.25	7.7	0.706869	±9.6	1
1.70	5254	−8.58	0.40	14	0.706867	±11	1
1.80	5308	−8.59	0.22	7.2	–	–	
2.00	5435	−8.88	0.20	5.6	0.706869	±6.6	1
2.20	5575	−8.79	0.22	6.5	0.706867	±6.0	1
2.40	5716	−9.02	0.25	7.6	0.706868	±6.0	1
2.60	5857	−9.18	0.30	9.6	0.706880	±6.2	1
2.90	6020	−9.06	0.18	4.8	0.706885	±6.4	1
3.10	6082	−9.74	0.19	5.4	0.706899	±7.8	1
3.30	6144	−9.50	0.21	5.5	0.706870	±11	1
3.50	6206	−9.32	0.20	5.6	0.706884	±8.4	1
3.70	6268	−9.69	0.33	10	0.706883	±10	1
3.90	6330	−9.52	0.27	9.3	0.706880	±6.4	1
4.10	6412	−9.07	0.22	6.2	0.706889	±6.2	1
4.30	6495	−9.70	0.22	6.5	0.706881	±6.6	1
4.50	6577	−9.62	0.29	9.2	0.706881	±6.6	1
4.70	6659	−9.59	0.18	7.1	0.706852	±15	2
4.90	7019	−8.74	0.23	6.0	0.706883	±6.6	1
5.00	7199	−8.61	0.31	8.7	0.706882	±9.4	1
5.15	7521	−8.90	0.38	19	0.706902	±14	2
5.25	7650	−8.49	0.24	7.8	0.706882	±13	2
5.30	7739	−8.41	0.29	11	0.706879	±6.8	1
Hiatus 1							
5.60	10,787	−4.68	0.36	13	0.706889	±6.0	1
5.85	10,814	−7.83	0.41	14	0.706883	±6.6	1
6.05	10,835	−7.66	0.34	9.6	–	–	
6.15	10,960	−7.57	0.36	12	0.706870	±5.8	1
6.20	11,043	−7.19	0.19	6.2	0.706906	±15	2
6.30	11,169	−8.42	0.25	8.3	0.706888	±15	2
6.40	11,267	−8.40	0.18	5.8	0.706890	±15	2
6.50	11,430	−8.21	0.23	6.0	–	–	
Hiatus 2							
6.60	12,766	−5.79	0.24	7.1	0.706883	±14	2
6.65	12,790	−5.63	0.29	7.5	0.706883	±5.8	1
6.80	12,862	−6.39	0.26	9.0	0.706895	±12	2
6.90	12,993	−7.56	0.27	10	0.706861	±15	2
7.00	13,391	−7.66	0.21	6.6	0.706921	±19	2
7.05	13,466	−7.83	0.39	15	0.706893	±7.2	1
7.15	13,617	−7.97	0.31	14	0.706895	±16	2
7.20	13,635	−7.64	0.37	13	0.706889	±5.4	1
7.30	13,643	−7.87	0.34	14	0.706888	±15	2
7.45	13,680	−7.76	0.31	11	0.706909	±15	2
7.60	14,000	−7.67	0.30	11	0.706892	±17	2
7.70	14,369	−7.29	0.27	8.6	0.706889	±15	2
7.80	14,668	−7.06	0.43	13	0.706890	±14	2
7.90	14,976	−5.11	0.50	17	0.706891	±7.0	1
8.10	15,669	−6.07	0.35	12	0.706892	±15	2
8.20	15,793	−7.05	0.28	9.6	0.706902	±13	2
8.30	15,882	−7.25	0.37	11	0.706897	±8.6	1
8.70	16,101	−5.98	0.43	13	0.706892	±6.0	1
8.90	16,234	−5.46	0.42	14	0.706895	±7.4	1
9.10	16,358	−5.07	0.37	11	0.706893	±6.4	1
9.30	16,476	−5.86	0.37	12	0.706901	±8.6	1
9.90	16,749	−6.05	0.41	11	0.706889	±6.6	1
10.1	16,786	−5.17	0.36	11	0.706895	±8.2	1
10.3	16,827	−5.29	0.40	11	0.706900	±8.6	1
10.5	16,875	−5.71	0.38	11	0.706920	±4.6	1
10.7	16,922	−5.21	0.41	11	0.706894	±8.8	1
10.9	16,970	−5.32	0.46	14	0.706897	±8.8	1
11.1	17,020	−5.38	0.43	13	0.706893	±7.6	1
11.3	17,072	–5.16	0.44	13	0.706893	±6.6	1
11.5	17,123	−4.70	0.44	14	0.706904	±6.4	1
11.7	17,174	−5.29	0.55	16	0.706884	±6.4	1
11.9	17,259	−4.53	0.57	16	0.706893	±7.0	1
12.1	17,478	−4.48	0.42	13	0.706896	±7.0	1
12.3	17,697	−3.20	0.86	25	0.706890	±7.2	1
12.5	17,916	−3.39	0.48	14	0.706899	±6.2	1
12.6	18,025	−4.69	0.30	8.8	0.706900	±6.2	1

[a] The $\delta^{13}C$ value is the average of the original $\delta^{13}C$ values (Fig. 2) in each interval for the trace element analysis.
[b] Subscripts 1 and 2 indicate the institute where isotopic ratios were analyzed, KCC and NCKU, respectively.

higher than the values for Hiro-1. The $\delta^{13}C$ values of the eight limestone specimens collected near the cave vary from −0.51‰ to 2.30‰, showing the average of 0.98‰ (Table 5).

The H_2O-leachates of the three andesite samples have Sr/Ca ratios of 1.0–1.8 mmol/mol and Ba/Ca of 0.05–0.09 mmol/mol (Table 4). Sr and Ba concentrations in the HOAc-leachates of andesites were three orders of magnitude higher than the H_2O-leachates, while the Me/Ca ratios (Sr/Ca = 1.3–2.1 mmol/mol with an average of 1.6 mmol/mol and Ba/Ca = 0.07–0.16 mmol/mol with an average of 0.10 mmol/mol) are only slightly higher than the ratios in the H_2O-leachates. The $^{87}Sr/^{86}Sr$ ratios of the HOAc-leachates range from 0.706302 to 0.706528 with an average of 0.706441, which is lower than the values for Hiro-1.

The modern dripwater samples, DW1 and DW2, showed similar Sr/Ca and Ba/Ca ratios that are in average 4.0 mmol/mol and 0.07 mmol/mol, respectively. The $^{87}Sr/^{86}Sr$ ratio of DW2 (0.706851; Table 4) is in a similar range as the Hiro-1 values, while the $^{87}Sr/^{86}Sr$ ratio of DW1 shows far lower value (0.706798).

4. Discussion

4.1. Isotopic mixing process

The $^{87}Sr/^{86}Sr$ ratios in Hiro-1 (average 0.706890) and the modern dripwater (average 0.706825) are between the ratios of two major rock types in the catchment area; limestone (0.707601 in average) and andesite (HOAc-leachate; 0.706441 in average) (Fig. 4 and Table 4). This indicates that the parent water of Hiro-1 requires a non-limestone Sr source with low-$^{87}Sr/^{86}Sr$ that mixes with limestone-derived Sr to decrease the $^{87}Sr/^{86}Sr$ ratio. Andesite, which is widely distributed in the cave, is the most likely low-$^{87}Sr/^{86}Sr$ strontium source. Atmospherically derived components, such as aeolian dust and sea salt (0.7109 and 0.70916, respectively; Palmer and Edmond, 1989; Yang et al., 2000) may be other potential Sr sources. However, the high $^{87}Sr/^{86}Sr$ ratios of such components are incompatible with the low $^{87}Sr/^{86}Sr$ ratios observed for Hiro-1. In addition, the Maboroshi Cave is located far from aeolian-dust source (Loess Plateau in central China) and from the coast. Thus, we conclude that the parental water of Hiro-1 is derived from two distinct strontium sources, limestone and andesite, and the contribution from the atmospherically derived sources was insignificant.

In order to evaluate source mixing processes, we examined a strontium isotopic mixing diagram, including all available $^{87}Sr/^{86}Sr$ data in this study versus the reciprocal Sr/Ca ratio (Fig. 4). In this diagram, the Sr/Ca ratios of the solid phases (X_{Sr}/X_{Ca}, for Hiro-1 and limestones) are converted to the ratios for the equilibrated aqueous phases ([Sr]/[Ca]) because the mixing process associated with stalagmite formation always takes place in aqueous phase. This conversion can be made as follows:

$$[Sr]/[Ca] = X_{Sr}/X_{Ca}/D_{Sr} \quad (1)$$

where square bracket and X represent the elemental concentrations given by mol/L and mol/g, respectively. The calcite/water distribution coefficient of strontium (D_{Sr}) is estimated from the Rimstidt et al. (1998),

Table 4
Sr/Ca and Ba/Ca molar fraction ratios and $^{87}Sr/^{86}Sr$ ratios in host limestones, wall-rock andesites and dripwaters.

Host		Sr/Ca solid mmol/mol	Ba/Ca solid μmol/mol	[Sr]/[Ca] water[a] mmol/mol	[Ba]/[Ca] water[a] mmol/mol	$^{87}Sr/^{86}Sr$	2SE × 10^{-6}
Limestones							
A1		0.18	6.9	1.7	0.28	0.707742	±6.4
A2		0.17	6.2	1.7	0.25	0.707830	±6.8
A3		0.18	7.5	1.7	0.31	0.707625	±6.4
B1		0.16	6.0	1.5	0.24	0.707699	±6.4
B2		0.17	5.5	1.6	0.22	0.707530	±6.2
B3		0.19	6.1	1.8	0.25	0.707423	±6.6
C1		0.13	6.7	1.2	0.27	0.707504	±6.6
C2		0.11	6.2	1.0	0.25	0.707636	±7.4
C3		0.14	6.4	1.3	0.26	0.707422	±6.6
Average		0.16	6.4	1.5	0.26	0.707601	
Andesites	Soaked by						
AN1	H_2O			1.8	0.09	–	–
AN2	H_2O			1.4	0.09	–	–
AN3	H_2O			1.0	0.05	–	–
AN1	HOAc			2.1	0.16	0.706528	±13
AN2	HOAc			1.9	0.15	0.706302	±22
AN3	HOAc			1.3	0.07	0.706494	±14
Average				1.6	0.10	0.706441	
Dripwater							
DW1				4.5	0.08	0.706798	±5.8
DW2				3.5	0.07	0.706851	±6.4

[a] Sr/Ca and Ba/Ca ratios for host limestone are calculated assuming chemical equilibrium between the water and the limestone.

where the D_{Sr} value is expressed as a function of the thermodynamic solubility products (K) of $CaCO_3$ and $SrCO_3$ as:

$$D_{Sr} = 0.022\left(\frac{K_{CaCO_3}}{K_{SrCO_3}}\right)^{0.57}. \quad (2)$$

Parameters used in the model calculations are listed in Table 6. Given the current average temperature in the Maboroshi cave (11 °C; Shen et al., 2010), the D_{Sr} value is estimated to be 0.105. Using the X_{Sr}/X_{Ca} ratio of the average value of limestone (0.16 mmol/mol), we obtain a [Sr]/[Ca] ratio of 1.5 mmol/mol for the water equilibrated with the limestone. For the andesite source, we use the values for the HOAc-leachates because we regard these values as representative of dissolved cations derived from leaching by weakly acidic soil water. The [Sr]/[Ca] ratios of dripwater equilibrated with Hiro-1 stalagmite are estimated to be 1.5 to 7.7 mmol/mol using Eqs. (1) and (2).

Because of the relatively homogeneous $^{87}Sr/^{86}Sr$ ratios, plots for the dripwater in equilibrium with Hiro-1 form a nearly vertical array, and importantly, intersect with the mixing line of the waters derived from the host limestone and from the andesite at the low [Sr]/[Ca] end (Fig. 4a). This suggests that the [Sr]/[Ca] ratio of the water had been largely increased from the original value before dripping onto Hiro-1 (discussed in the next section), and that the proportion of two Sr sources (limestone and andesite) was relatively stable over the growth period of Hiro-1. The relative proportion of the two sources can be evaluated from the Sr isotopic mass balance as:

$$\left({}^{87}Sr/{}_{86}Sr_{lim}\right)\times\left(\frac{[Sr]}{[Ca]}\right)_{lim}\times a + \left({}^{87}Sr/{}_{86}Sr_{ads}\right)\times\left(\frac{[Sr]}{[Ca]}\right)_{ads}\times(1-a) = \left({}^{87}Sr/{}_{86}Sr\right)_{mix}\times\left(\frac{[Sr]}{[Ca]}\right)_{mix} \quad (3)$$

where a indicates the proportion of limestone source ($0 < a < 1$), and the subscripts "lim", "ads" and "mix" refer the waters derived from host limestone, andesite, and mixture, respectively. When we use the average $^{87}Sr/^{86}Sr$ and [Sr]/[Ca] ratios calculated for the waters equilibrated with the limestone and the andesite (Table 4), and adopt the isotopic ratios of Hiro-1 (Table 3) as the $(^{87}Sr/^{86}Sr)_{mix}$ values, the proportion of the limestone source, a, is estimated between 0.36 and 0.43 with an average of 0.40. A slight decrease of the a values is seen from HS1 to the middle Holocene (Fig. 5b).

Modern dripwater samples, DW1 and DW2, show lower $^{87}Sr/^{86}Sr$ ratios than those of Hiro-1 (Fig. 4a), indicating a larger contribution of the andesite source than during the growth period of Hiro-1.

4.2. Prior calcite precipitation

The [Sr]/[Ca] ratio of water equilibrated with Hiro-1 stalagmite is obviously higher than that expected for a simple mixing of waters equilibrated with limestone and andesite (Fig. 4a). This relative enrichment of Sr is most likely caused by PCP, calcite precipitation from the infiltrating water prior to the stalagmite formation. This process can be examined using Ba, which also has a distribution coefficient smaller than 1 (Rimstidt et al., 1998). Our age profile for Hiro-1 shows the coherent variation in Ba/Ca and Sr/Ca ratios (Fig. 3). Here, we examine the effect of PCP using a Rayleigh-type fractionation model, following Johnson et al. (2006).

PCP takes place during transit of water in aerated channels in the limestone aquifer before a stalagmite forms. Water containing high concentrations of dissolved carbonate species becomes supersaturated with calcium carbonate when CO_2 degasses from the water. Calcite precipitation selectively uptakes Ca from the water relative to the other alkaline earth metals such as Sr and Ba.

We assume that the [Me]/[Ca] increases during successive calcite precipitation following the Rayleigh distillation equation;

$$\ln\left(\frac{{}^{[Me]}/_{[Ca]}}{\left({}^{[Me]}/_{[Ca]}\right)_0}\right) = (D_{Me}-1)\ln f \quad (4)$$

Table 5
The $\delta^{13}C$ values (‰ VPDB) of eight limestone samples collected from the catchment area of the Maboroshi cave.

Sample name	Mb01	Mb02	Mb03	Mb04	Mb05	Mb06	Mb07	Mb08	Average
$\delta^{13}C$ values (‰ VPDB)	2.15	1.93	2.30	1.79	0.00	0.61	−0.39	−0.51	0.98

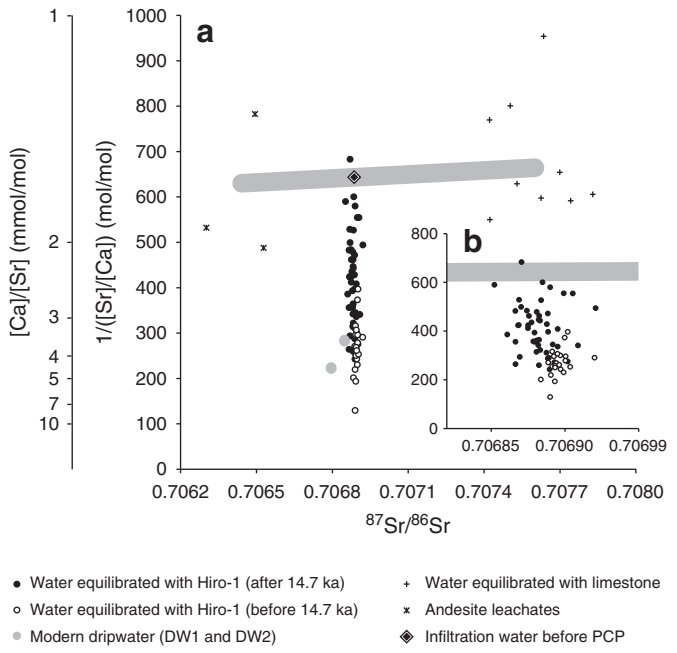

Fig. 4. (a) A cross plot of 1/([Sr]/[Ca]) versus $^{87}Sr/^{86}Sr$ ratios. The [Sr]/[Ca] of limestone and Hiro-1 indicates the ratios of waters equilibrated with solid phase. Gray thick line connects two average plots of limestone and andesite. (b) Plots with an enlarged horizontal axis.

where $([Me]/[Ca])_0$ is the molar concentration ratio of Sr or Ba to Ca in the initial water with the proportions of the two sources ($a = 0.35$–0.45) estimated from $^{87}Sr/^{86}Sr$. The $([Sr]/[Ca])_0$ ratio is estimated to be 1.6 mmol/mol. For Ba, we adopted a distribution coefficient D_{Ba} of 0.025 at 11 °C (Table 5), the limestone X_{Ba}/X_{Ca} ratio of 6.4 μmol/mol and the [Ba]/[Ca] ratio of andesite leachate of 0.10 mmol/mol, resulting in the initial ratio, $([Ba]/[Ca])_0$ of 0.16 mmol/mol. The variable f represents the molar ratio of residual to initial Ca^{2+} concentration in the water ($[Ca]/[Ca]_0$), and the degree of PCP can be expressed as $1 - f$.

A similar model can be used for $\delta^{13}C$ values during PCP. PCP results in a positive shift in stalagmite $\delta^{13}C$ because of the preferential removal of $^{12}CO_2$ from the infiltrating water. Because the equilibrium carbon isotopic fractionation between dissolved carbon species and calcite is insignificant (Emrich et al., 1970), we simply use the stalagmite $\delta^{13}C$ as that of the dissolved carbon species of dripwater. Assuming the isotopic equilibrium both for CO_2 degassing and calcite precipitation, the Rayleigh-type fractionation for $\delta^{13}C_{HCO3-}$ can be expressed as;

$$\delta^{13}C_{HCO3-} - \delta^{13}C^{0}_{HCO3-} = -\frac{\epsilon}{1 + {}^{\epsilon}/_{1000}} \cdot \ln f \quad (5)$$

where ε is the carbon isotopic fractionation between bicarbonate and gaseous CO_2, and estimated to be 9.23 at 11 °C (Zhang et al., 1995). Assuming limestone dissolution in an ideal closed system (Hendy, 1971), the $\delta^{13}C^{0}_{HCO3-}$ value is calculated as −13‰ by 1:1 mixing of soil CO_2 from C3 vegetation cover (typically −26 to −28‰) and carbonate carbon (about 1‰, Table 5) as simply expressed by

$$CaCO_3 + CO_2(soil) + H_2O \rightarrow Ca^{2+} + 2HCO_3^- \quad (6)$$

Our previous observations in karst groundwaters near the Maboroshi Cave, where the measured $\delta^{13}C$ in soil CO_2 was approximately −25‰, gave a range of −14 to −12‰ for $\delta^{13}C_{HCO3-}$ (Hori et al., 2008). This range is near the estimate here, and therefore a value of −13‰ for $\delta^{13}C^{0}_{HCO3-}$ is likely appropriate.

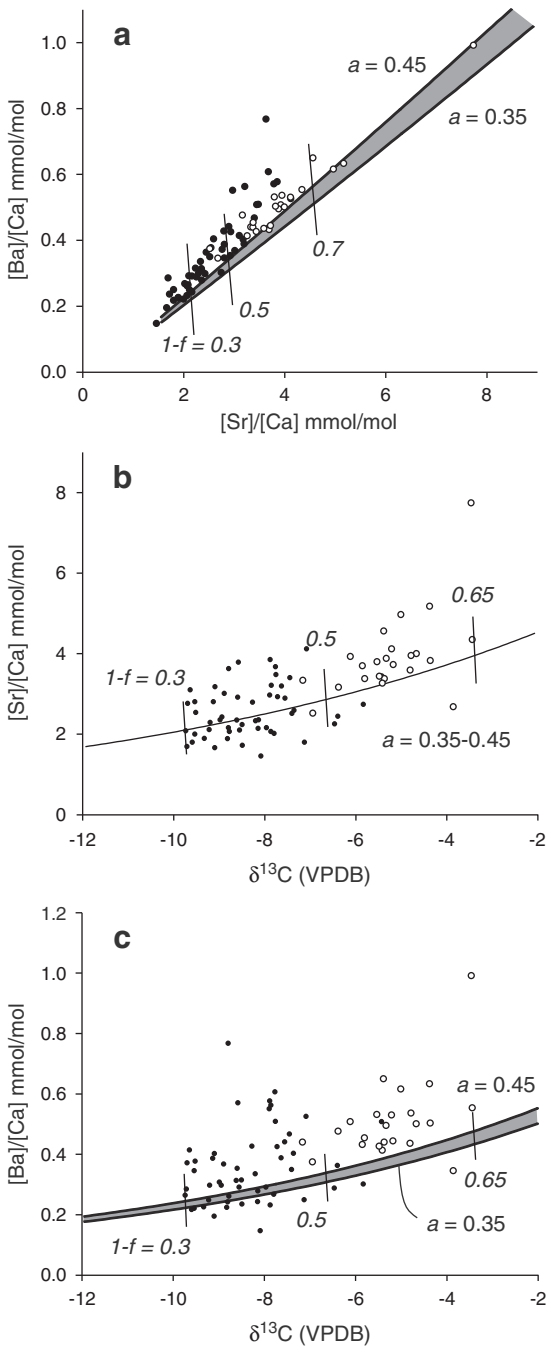

Fig. 5. Cross plots showing the chemical evolution of parental water for Hiro-1 by PCP: (a) [Ba]/[Ca] versus [Sr]/[Ca] ratios, (b) [Sr]/[Ca] ratio versus $\delta^{13}C$ values and (c) [Ba]/[Ca] ratio versus $\delta^{13}C$ values. Open and solid circles indicate the data before and after 14.7 ka, respectively. Curves with gray area represent the calculated Rayleigh-type evolution with the proportions of limestone and andesite sources ($a = 0.35$–0.45). Thin line with italic number shows the degree of PCP ($1 - f$).

Table 6
Solubility products of carbonate minerals, distribution factors of Ca, Sr and Ba between water and calcite, and carbon isotopic fractionation factors between bicarbonate and gaseous CO_2 used in the calculation of this study.

$logK_{CaCO3}$ [a]	$logK_{SrCO3}$	$logK_{BaCO3}$	D_{Sr}	D_{Ba}	ε
−8.31	−9.50	−8.40	0.105	0.025	9.23

[a] $logK_{CaCO3} = 9.72 - 2378 \times T(°K) - 0.0340 / T(°K)$, $\log K_{SrCO3} = 13.02 - 3565 \times T(°K) - 0.0351 / T(°K)$, $\log K_{BaCO3} = 12.94 - 3269 \times T(°K) - 0.0346 / T(°K)$ by Naumov et al. (1974), where T was fixed as 11 °C.

Fig. 5 shows cross-plots for [Sr]/[Ca]–[Ba]/[Ca] (a), δ^{13}C–[Sr]/[Ca] (b) and δ^{13}C–[Ba]/[Ca] (c). In all cases, the data are broadly distributed along a Rayleigh-type evolution curve. Therefore, we conclude that these three variables have been largely controlled by successive PCP. However, the Hiro-1 data tend to plot above the calculated evolution curve in two diagrams of [Sr]/[Ca]–[Ba]/[Ca] (Fig. 5a) and δ^{13}C–[Ba]/[Ca] (Fig. 5c). This discrepancy between the observed data and the modeled values implies that an additional factor is involved in determining the [Ba]/[Ca] ratio. One possible factor is kinetic effects, that is, the influence of crystal growth rate on trace element incorporation. It has been demonstrated for stalagmites that the apparent distribution coefficient of alkaline earth metals, including Ba and Sr, generally increases with the growth rate (e.g., Tesoriero and Pankow, 1996). Ba might have a higher growth rate-dependence than Sr as revealed in high-resolution geochemical profiles in a stalagmite from southwest Australia (Treble et al., 2003). The kinetic effect may even influence stalagmite δ^{13}C values (e.g., Frisia et al., 2011), but this effect has not been fully understood. In the case of Hiro-1, it seems that kinetic effects have a greater influence for Ba than for Sr and δ^{13}C.

Although our Rayleigh-type model slightly underestimates the Ba values, PCP explains the overall trend of the Hiro-1 data (Fig. 5). Here, we estimate the degree of PCP ($1 - f$) of Hiro-1 on the basis of Sr/Ca–Ba/Ca ratios and δ^{13}C (Fig. 6). The element-based estimate gives larger variation of PCP than the δ^{13}C-based estimation. The $1 - f$ values are high throughout HS 1 (75–50% in element-base, and 60–50% in δ^{13}C-base), and gradually decrease toward the middle Holocene (60–10% in element-base, and around 40% in δ^{13}C-base; Fig. 6).

4.3. Relationship between the proxy record and paleoclimate in 18.0–4.5 ka

The Sr/Ca and Ba/Ca ratios and δ^{13}C values in Hiro-1 vary depending on the degree of PCP over the growth period, which is likely to be influenced by climate conditions, such as rainfall intensity (Fairchild et al., 2000; Johnson et al., 2006). In this study, we compare the degree of PCP with δ^{18}O records (Fig. 6).

The degree of PCP gradually decreases along with the δ^{18}O values from HS1 to the middle Holocene excepting the periods of the stalagmite growth termination. The HS1 is understood as a cold and dry climate period in the East Asian Monsoon region (e.g., Wang et al., 2001), and the coupled influence from low temperature and low precipitation was responsible for the more positive δ^{18}O values of Hiro-1 during this period (Fig. 2). Dryness during the HS1 also accounts for the high degree of PCP ($1 - f = 0.7$; Fig. 6). An abrupt decrease of humidity was also suggested immediately before Hiatus 1, where positive δ^{18}O values and high degree of PCP (~60%; Fig. 6) are recorded. Termination of the stalagmite growth may have been related with the decreased rainfall amount that could not feed dripwater to Hiro-1. In the middle Holocene, the element-based ($1 - f$) value largely fluctuated between 10 and 65%, and reached ~0% in 4.6 ka (Fig. 6). This suggests that the climate became more humid, consistent with previous studies on pollen records of terrestrial sediments in SW Japan indicating the humid (and warm) climate of this period (Gotanda and Yasuda, 2008; Hase et al., 2011). Modern dripwater shows significantly evolved [Sr]/[Ca] ratios of 3.5 to 4.5 mmol/mol (or low 1 / ([Sr]/[Ca]) ratio of 220–280 mol/mol; Fig. 4), suggesting that the current conditions are again as dry as the last glacial period.

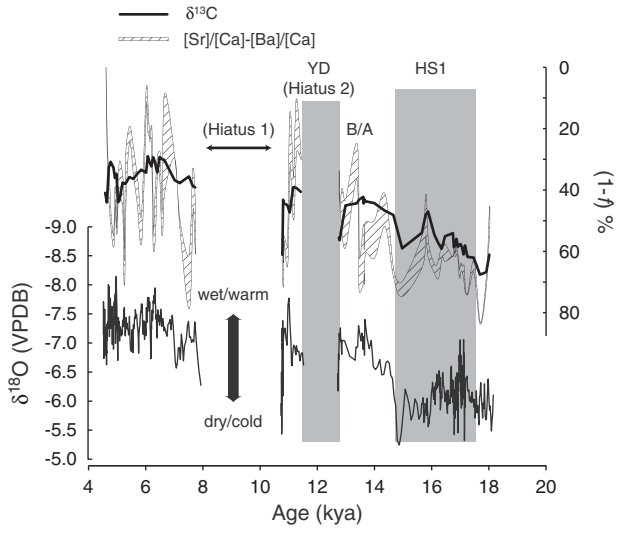

Fig. 6. Age profiles of δ^{18}O values and degrees of prior precipitation of calcite ($1 - f$) for Hiro-1. Degrees of prior precipitation of calcite, ($1 - f$), were calculated on the basis of [Sr]/[Ca]–[Ba]/[Ca] and δ^{13}C values.

Finally, we discuss the origin of general decreasing trend of ^{87}Sr/^{86}Sr ratio with age (Fig. 3), which suggests the increase of andesite-derived components. It is likely that the erosion of andesite was controlled by chemical weathering process. Previous studies have suggested that warm and humid climates accelerate weathering rates relative to cold and dry climates (e.g., Lasaga et al., 1994; White and Blum, 1995). Silicate weathering rates may increase with partial pressure of CO_2 (pCO_2) in soils (Kump et al., 2000; Assayag et al., 2009), although high pCO_2 simultaneously enhances carbonate dissolution. The combined effects of increasing temperature, humidity, and soil pCO_2 during the Holocene are likely to intensify andesite weathering. The lowest ^{87}Sr/^{86}Sr ratios were observed in 5.7–5.2 ka (Fig. 3) and in the modern dripwater (Fig. 4a). It is plausible that recent climate change has resulted in andesite weathering rates reaching some of the most rapid rates during the Holocene.

As discussed above, the Sr/Ca and Ba/Ca ratios of Hiro-1 are predominantly controlled by Rayleigh-type successive PCP, while the ^{87}Sr/^{86}Sr ratios reflect mixing of the two major sources (limestone and andesite). Increasing humidity toward the middle Holocene may be responsible for both of decreasing PCP (Fig. 6) and increasing contribution of andesite-derived Sr (Fig. 4b). It is noteworthy that the Me/Ca ratios of karst water reflects humidity change when the proportion of Me sources is relatively constant. Our results show a significant influence from PCP to stalagmite Me/Ca ratios that record long-term humidity change, as supported by the covariance between PCP and δ^{18}O (Fig. 6).

5. Summary

We analyzed Sr/Ca, Ba/Ca and ^{87}Sr/^{86}Sr ratios in a stalagmite from southwest Japan (Hiro-1) covering the interval 18.0–4.5 ka. We examined the influence of two distinct processes (prior calcite precipitation and source mixing) on the Sr/Ca, Ba/Ca and ^{87}Sr/^{86}Sr ratios of the stalagmite.

(1) *Source mixing process*. The relatively homogeneous ^{87}Sr/^{86}Sr ratios throughout the stalagmite (0.706852–0.706921) require a constant mixing ratio between two major Sr sources of the catchment area (limestone and andesite). Assuming these end-components, 57–64% of Sr was derived from andesite (average 0.706441) and the remaining Sr was originated from limestone (average 0.707601). The maximum contribution of the andesite-derived Sr component is observed in the middle Holocene (5.7–5.2 ka). The increase of the andesite-derived component may have resulted from increasing chemical weathering rate in the karst system under relatively higher temperature, humidity and higher pCO_2 in soil layer.

(2) *Prior calcite precipitation (PCP)*. Sr/Ca and Ba/Ca ratios of the stalagmite were much higher than those expected from the initial water, implying a significant role of PCP. This was supported by Sr/Ca, Ba/Ca and δ^{13}C values of Hiro-1, which broadly follow the Rayleigh-type fractionation model of PCP (Fig. 5), although

kinetic effect might have played an additional role, especially for enrichment of Ba. The degree of PCP is evaluated as 0 to 85% based on elemental ratios (Figs. 5 and 6), and generally decreases from the last glacial maximum (18 ka) to the middle Holocene (4.6 ka). The largest degree of PCP observed during the HS1 may have reflected a drier climate during this period. PCP can be a major process controlling the trace elemental composition of stalagmites. Evaluation of the effects from PCP is valuable when we reconstruct the paleoenvironmental changes on the basis of stalagmite data.

Acknowledgments

We thank Mr. Yozou Tsuchiya, manager of Maboroshi cave, for supporting sampling in the cave. Dr. I. Fairchild and two anonymous reviewers provided valuable comments for improving the manuscript. U–Th isotopic measurements for ^{230}Th dating were supported by NSC and NTU grants (NSC 99-2611-M-002-006, 99-2628-M-002-012, and 101R7625 to C.C.S.). Fieldwork in the Maboroshi Cave was supported by JSPS grant (21340149 to A.K.).

Appendix A. Supplementary data

Supplementary data to this article can be found online at http://dx.doi.org/10.1016/j.chemgeo.2013.03.005.

References

Alley, R.B., Messe, D.A., Shuman, C.A., Gow, A.J., Taylor, K.C., Grootes, P.M., White, J.W.C., Ram, M., Waddington, E.D., Mayewski, P.A., Zielinski, G.A., 1993. Abrupt increase in Greenland snow accumulation at the end of the Younger Dryas event. Nature 362, 527–529.

Assayag, N., Matter, J., Ader, M., Goldberg, D., Agrinier, P., 2009. Water-rock interactions during a CO_2 injection field-test: Implications on host rock dissolution and alteration effects. Chemical Geology 265, 227–235.

Ayalon, A., Bar-Matthews, M., Kaufman, A., 1999. Petrography, strontium, barium and uranium concentrations, and strontium and uranium isotope ratios in speleothems as paleoclimatic proxies: Soreq Cave, Israel. The Holocene 9, 715–722.

Banner, J.L., Musgrove, W.L., Asmeron, Y., Edwards, R.L., Hoff, J.A., 1996. High-resolution temporal record of Holocene ground-water chemistry: tracing links between climate and hydrology. Geology 24, 1049–1053.

Barker, S., Diz, P., Vautravers, M.J., Pike, J., Knorr, G., Hall, I.R., Broecker, W.S., 2009. Interhemispheric Atlantic seesaw response during the last deglaciation. Nature 457, 1097–1103.

Broecker, W., Barker, S., 2007. A 190‰ drop in atmosphere's $\Delta^{14}C$ during the "Mystery Interval" (17.5 to 14.5 kyr). Earth and Planetary Science Letters 256, 90–99.

Cheng, H., Edwards, R.L., Hoff, J., Gallup, C.D., Richards, D.A., Asmerom, Y., 2000. The half-lives of uranium-234 and thorium-230. Chemical Geology 169, 17–33.

Dansgaard, W., 1964. Stable isotopes in precipitation. Tellus 16, 436–438.

Emrich, K., Dhhalt, D.H., Vogel, J.C., 1970. Carbon isotope fractionation during the precipitation of calcium carbonate. Earth and Planetary Science Letters 8, 363–371.

Fairchild, I.J., Treble, P.C., 2009. Trace elements in speleothems as recorders of environmental change. Quaternary Science Reviews 28, 449–468.

Fairchild, I.J., Borsato, A., Tooth, A.F., Frisia, S., Hawkesworth, C.J., Huang, Y., McDermott, F., 2000. Controls on trace element (Sr–Mg) compositions of carbonate cave waters: implications for speleothem climatic records. Chemical Geology 166, 255–269.

Fairchild, I.J., Smith, C.L., Baker, A., Fuller, L., Spötl, C., Mattey, D., McDermott, F., E.I.M.F., 2006. Modification and preservation of environmental signals in speleothems. Earth-Science Reviews 75, 105–153.

Frisia, S., Fairchild, I.J., Fohlmeister, J., Miorandi, R., Spötl, C., Borsato, A., 2011. Carbon mass-balance modelling and carbon isotope exchange processes in dynamic caves. Geochimica et Cosmochimica Acta 75, 380–400.

Goede, A., McCulloch, M., McDermott, F., Hawkesworth, C., 1998. Aeolian contribution to strontium and strontium isotope variations in a Tasmanian speleothem. Chemical Geology 149, 37–50.

Gotanda, K., Yasuda, Y., 2008. Spatial biome changes in southwestern Japan since the Last Glacial Maximum. Quaternary International 184, 84–93.

Hase, Y., Iwauchi, A., Uchikoshiyama, U., Eguchi, E., Sasaki, N., 2011. Vegetation changes after the late period of the last glacial age based on pollen analysis of the northern area of Aso Caldera in central Kyushu, southwest Japan. Quaternary International 254, 107–117.

Hendy, C.H., 1971. The isotopic geochemistry of speleothems: the calculations of the effects of different modes of formation on the isotopic composition of speleothems and their applicability as palaeoclimate indicators. Geochimica et Cosmochimica Acta 35, 801–824.

Hori, M., Hoshino, K., Okumura, K., Kano, A., 2008. Seasonal patterns of carbon chemistry and isotopes in tufa depositing groundwaters of southwestern Japan. Geochimica et Cosmochimica Acta 72, 480–492.

Hori, M., Takashima, C., Matsuoka, J., Kano, A., 2009. Carbon and oxygen stable isotopic measurements of carbonate and water samples using mass spectrometer with gas bench. (in Japanese) B. Grad. Sch. Cult. Stud. Kyushu University 15, 51–57.

Horwitz, E.Ph., Dietz, M.L., Chiarizia, R., 1992. The application of novel extraction chromatographic materials to the characterization of radioactive waste solutions. Journal of Radioanalytical and Nuclear Chemistry 161, 575–583.

Jaffey, A.H., Flynn, K.F., Glendenin, L.E., Bentley, W.C., Essling, A.M., 1971. Precision measurement of half-lives and specific activities of ^{235}U and ^{238}U. Physics Review 4, 1889–1906.

Johnson, K.R., Hu, C., Belshaw, N.S., Henderson, G.M., 2006. Seasonal trace-element and stable-isotope variations in a Chinese speleothem: the potential for high-resolution paleomonsoon reconstruction. Earth and Planetary Science Letters 244, 394–407.

Kump, L.R., Brantley, S.L., Arthur, M.A., 2000. Chemical weathering, atmospheric CO_2, and climate. Annual Review of Earth and Planetary Sciences 28, 611–667.

Lachniet, M.S., 2009. Climatic and environmental controls on speleothem oxygen-isotope values. Quaternary Science Reviews 28, 412–432.

Lasaga, A.C., Soler, J.M., Ganor, J., Burch, T.E., Nagy, K.L., 1994. Chemical weathering rate laws and global geochemical cycles. Geochimica et Cosmochimica Acta 58, 2361–2386.

McDermott, F., 2004. Palaeo-climate reconstruction from stable isotope variations in speleothems: a review. Quaternary Science Reviews 23, 901–918.

Naumov, G.B., Ryzhenko, B.N., Kodakovsky, I.L., 1974. Handbook of thermodynamic data. N.T.I.S report number USGS-WRD-74-001.

Nümberg, D., Bijma, J., Hemleben, C., 1996. Assessing the reliability of magnesium in foraminiferal calcite as a proxy for water mass temperatures. Geochimica et Cosmochimica Acta 60, 803–814.

Palmer, M.R., Edmond, J.M., 1989. The strontium isotope budget of the modern ocean. Earth and Planetary Science Letters 92, 11–26.

Rimstidt, J.D., Balog, A., Webb, J., 1998. Distribution of trace elements between carbonate minerals and aqueous solutions. Geochimica et Cosmochimica Acta 62, 1851–1863.

Shen, C.-C., Lee, T., Chem, C.-Y., Wang, C.-H., Dai, C.-F., Li, L.-A., 1996. The calibration of *D*[Sr/Ca] versus sea surface temperature relationship for *Prites* corals. Geochimica et Cosmochimica Acta 60, 3849–3858.

Shen, C.-C., Edwards, R.L., Cheng, H., Dorale, J.A., Thomas, R.B., Moran, S.B., Weinstein, S.E., Edmonds, H.N., 2002. Uranium and thorium isotopic and concentration measurements by magnetic sector inductively coupled plasma mass spectrometry. Chemical Geology 185, 165–178.

Shen, C.-C., Cheng, H., Edwards, R.L., Moran, S.B., Edmonds, H.N., Hoff, J.A., Thomas, R.B., 2003. Measurement of attogram quantities of ^{231}Pa in dissolved and particulate fractions of seawater by isotope dilution thermal ionization mass spectroscopy. Analytical Chemistry 75, 1075–1079.

Shen, C.-C., Kano, A., Hori, M., Lin, K., Chiu, T.-C., Burr, G.S., 2010. East Asian monsoon evolution and reconciliation of climate records from Japan and Greenland during the last deglaciation. Quaternary Science Reviews 29, 3327–3335.

Shen, C.-C., Wu, C.-C., Cheng, H., Edwards, R.L., Hsieh, Y.-T., Gallet, S., Chang, C.-C., Li, T.-Y., Lam, D.D., Kano, A., Hori, M., Spötl, C., 2012. High-precision and high-resolution carbonate ^{230}Th dating by MC-ICP-MS with SEM protocols. Geochimica et Cosmochimica Acta 99, 71–86.

Tesoriero, A.J., Pankow, J.F., 1996. Solid solution partitioning of Sr^{2+}, Ba^{2+}, and Cd^{2+} to calcite. Geochimica et Cosmochimica Acta 60, 1053–1063.

Tooth, A.F., Fairchild, I.J., 2003. Soil and karst aquifer hydrological controls on the geochemical evolution of speleothem-forming drip waters, Crag Cave, southwest Ireland. Journal of Hydrology 273, 51–68.

Treble, P., Shelley, J.M.G., Chappell, J., 2003. Comparison of high resolution sub-annual records of trace elements in a modern (1911–1992) speleothem with instrumental climate data from southwest Australia. Earth and Planetary Science Letters 216, 141–153.

Wang, Y.J., Cheng, H., Edwards, R.L., An, Z.S., Wu, J.Y., Shen, C.-C., Dorale, J.A., 2001. A high-resolution absolute-dated late Pleistocene monsoon record from Hulu cave, China. Science 294, 2345–2348.

Wang, Y.J., Cheng, H., Edwards, R.L., Kong, X., Shao, X., Chen, S., Wu, J.Y., Jiang, X., Wang, X.F., An, Z.S., 2008. Millennial- and orbital-scale changes in the East Asian monsoon over the past 224,000 years. Nature 451, 1090–1093.

White, A.F., Blum, A.E., 1995. Effects of climate on chemical weathering in watersheds. Geochimica et Cosmochimica Acta 59, 1729–1747.

Yang, J., Chen, J., An, Z., Shields, G., Tao, X., Zhu, H., Ji, J., Chen, Y., 2000. Variations in $^{87}Sr/^{86}Sr$ ratios of calcites in Chinese loess: a proxy for chemical weathering associated with the East Asian summer monsoon. Palaeogeography Palaeoclimatology Palaeoecology 157, 151–159.

Yokoo, Y., Nakano, T., Nishikawa, M., Quan, H., 2004. Mineralogical variation of Sr–Nd isotopic and elemental compositions in loess and desert sand from the central Loess Plateau in China as a provenance tracer of wet and dry deposition in the northwestern Pacific. Chemical Geology 204, 45–62.

Zhang, J., Quay, P.D., Wilbur, D.O., 1995. Carbon isotope fractionation during gas–water exchange and dissolution of CO_2. Geochimica et Cosmochimica Acta 59, 107–114.

Zhou, H., Feng, Y.-X., Zhao, J.-X., Shen, C.-C., You, C.-F., Lin, Y., 2009. Deglacial variations of Sr and $^{87}Sr/^{86}Sr$ ratio recorded by a stalagmite from central China and their association with past climate and environment. Chemical Geology 268, 233–247.